Available online at www.sciencedirect.com
SCIENCE DIRECT
Polymer 46 (2005) 5406–5416
polymer
www.elsevier.com/locate/polymer

In situ gradient nano-scale fibril formation during polypropylene (PP)/polystyrene (PS) composite fine fiber processing

Qiang Xing[a], Meifang Zhu[a,*], Yiheng Wang[a], Yanmo Chen[a], Yu Zhang[a], J. Pionteck[b], H.J. Adler[c]

[a]*State Key Lab for Modification of Chemical Fiber and Polymer Materials, College of Material Science and Engineering, Donghua University, 1882 West Yan-an Road, Shanghai 200051, China*
[b]*Institute of Polymer Research Dresden, Hohe Street 6, D-01069 Dresden, Germany*
[c]*Institute of Macromolecular Chemistry and Textile Chemistry, Dresden University of Technology, Mommsenstr. 13, D-01069 Dresden, Germany*

Received 5 January 2005; received in revised form 6 March 2005; accepted 9 March 2005
Available online 27 April 2005

Abstract

The nano-scale dispersed fibrils with gradient distribution in PP/PS composite fine fibers were observed by in situ formation during its melt spinning process. The morphology development of polyblends, from granule to as-spun fiber as well as drawn fiber with various PS content from 2 to 8 wt% were investigated. The morphology conversion of PS dispersed phase from ellipse to gradient nano-scale fibril along the radial direction of as-spun composite fibers took palace at 4 wt% by weight of PS component, suggesting the presence of break-up in fiber center and the limited coalescence, especially in 8 wt% PS as-spun composite fibers. This morphology diversity was attributed to the radial variation of parameters including temperature, viscosity, axial velocity and stress in spinning path and was in good agreement with the droplet deformation criteria based on the reduced capillary number. In addition, the post hot-drawing process slightly influence the size and distribution of PS phase in cross-section of composite drawn fibers, while the rheological properties of PP, PS and polyblends were found to be correlated to the morphology of PP/PS composites.

Keywords: Nano-scale fibril; Polypropylene (PP)/polystyrene (PS) composite; Fiber

1. Introduction

During the last two decades, the formation of polymer blends that result in fibrillar phase morphology (FPM) has been extensively investigated. The focus has been on understanding the principles that lead to the formation of such morphology [1]. One of the most important procedures to reach this objective is to blend a thermoplastic polymer (TP) matrix with thermotropic liquid crystal polymers (TLCPs) [2,3]. TLCPs are able to deform into fibrillar structures, leading to the so-called 'in situ' composites with improved mechanical properties, especially elastic modulus and tensile strength. [4–6] FPM composites can be fabricated by different methods, such as injection molding, compression molding, extruded sheet, fiber spinning and film extrusion [7–9], which resulted in different morphology and degree of orientation.

Compared to the above mentioned methods, fiber spinning is the most conducive method to create fibril morphology because the elongational force field exiting in the spinning process is more effective than the shear force field existing in other processes [10]. However, the research activities in the field of the more complicated fiber processing have been rather limited. Lots of these investigations concerned the PET/TCLP blend fibers [11,12]. By contrast, only a few papers about PP composite fibers have been published to date, but PP is already wildly interesting to use as the matrix for in situ composites by extrusion and molding process [13] because of its several excellent properties coupled with a low price, which will be not discussed here. For PP composite fibers with fibrillar phase morphology, the spinning experiments can be divided two kinds, one is carried out on blends of PP and TLCP for in situ composite, the other is related to blends of PP and TP.

* Corresponding author. Tel.: +86 21 62379549; fax: +86 21 62194722.
E-mail address: zmf@dhu.edu.cn (M. Zhu).

0032-3861/$ - see front matter © 2005 Elsevier Ltd. All rights reserved.
doi:10.1016/j.polymer.2005.03.100

Sukananta P. et al. [14] studied the properties of as-spun and drawn monofilaments of PP/LC5000 in situ composite, and found the significant improvement of both tensile and dynamic mechanical properties, especially in the high temperature region. Qin Y. et al. [15–17] investigated the fibril morphology and blend fiber mechanical properties affected by concentration, extrusion conditions, drawing conditions and different kinds of LCP. In post-drawing, the LCP fibrils were split into short fragments and the fiber properties were improved with the increase in drawing temperature. In PP/TP composite fibers, several papers have been published, most particularly fibers are from PP/PA6 [18,19]. Kotek R. [19] reported the PA6 phase contained fibrils in PP blend as-spun fibers. And the blend composition and interfacial adhesion provided by the compatilibilizer were two important factors that influenced the PA6 fibril morphology and fibers properties. Takahashi [20] studied the physical properties of PP/PA6 fibers influenced by its morphology. Grof I. [21] investigated the structure-property relationship in modified polypropylene–polycaproamide fibers containing MAH grafted PP. Lyoo W. S. [22] used modified PET/PP blends for producing microfibers by extracting continuous phase. Microfibers obtained after extraction of the continuous phase from an immiscible blend have proven useful for making artificial leather for apparel and other textile products with novel properties.

However, little information is available in scientific literature that sheds light on the difference existing in the morphologies of the polyblend material prior to and after extrusion into fibers. Numerous investigations above mentioned in blend fibers are carried out for the relationships in spinning conditions, fibril morphology and mechanical properties et al. [11–21]. And the sizes of fibrils in matrix were micro or sub-micron scale, while nano-scale fibrils were not reported not only in the blend fibers but also in the other kinds of composites. In addition, for thick products such as in injection modeling, a skin-core effect could be observed, by which the oriented fibrils were exhibited near to the skin of the molded part while dispersed droplets were present in the core region [23]. Fredrich K. [24] also reported the similar morphology in PP/PA66 materials which were attributed to the shear distribution in injection modeling. However, the shape and distribution of fibrils in blend fibers were mostly neglected, especially in fine fiber with small diameter. In this work, these two parts, nano-scale fibril formation and its gradient distribution in fibers, will be discussed in detail.

According to our previous work on the PP/PS blend fibers, the presence of the PS improves the dyeability of PP fiber which was evidently affected by PS composition and the crystal structure [25]. Based on this investigation, the novel inner morphology of PP/PS fibers were studied in this study which will be used to set up the relationship to the properties of composite fibers, such as the dyeability and mechanical properties, in the further research work. The PP/PS composite fine fibers with in situ gradient nano-scale fibril morphology were prepared by using a two-step method. In the first step, PP and PS were melting blended in a twin-screw extruder to get granules. In the second step, the polyblends were extruded into as-spun fibers using melt-spinning equipment. And the drawn composite fibers were obtained after the post-drawing. The different morphology of dispersed phase in PP matrix at each step was examined by SEM and theoretically analyzed with the results from image analyzer. The evaluation and the distribution of PS fibrils during fiber processing and its relationship with blend ratio and component properties were investigated.

2. Experimental

2.1. Materials

The type of PP raw material used was commercial isotactic polypropylene supplied by Donghua University, with a melt flow index (MFI) between 30.0 and 40.0 g/10 min (230 °C, 2.16 kg). Polystyrene was synthesized in our laboratory by suspension polymerization [26], with MFI of 50.0 g/10 min (230 °C, 2.16 kg).

2.2. Specimen preparation

The polypropylene and polystyrene were dried prior to mixing and melt blending of PP/PS at different weight ratio (98/2; 96/4; 94/6; 92/8 wt/wt) by twin-screw extruder (SH-35 co-rotating twin-screw extruder), immediately quenched in water, and then cut into granules by a pelletizer. In the extruding step, barrel temperatures were set at 180/200/210/220/195 °C, respectively, and a screw speed of 100 rpm was used. The *L*/*D* ratio of the screws was 30, and $D = 35$ mm.

The PP/PS composite as-spun fibers were prepared on an ABE Spinner Instrument (ABE Corp., Japan) at 260 °C with take-up velocity of 800 m/min. The spinneret had 60 holes with a diameter of 0.25 mm. Fibers were extruded at a constant throughput rate 16 g/min from the melt at 260 °C to the air at 25 °C. The as-spun fibers were hot drawn to get the drawn fibers using Barmag 3010 Drawer (BARMAG, Germany) set to 70 °C for the heat roller and to 100 °C for the winding roller. And the drawn ratio was controlled by the speed ratio of winding and heat roller.

2.3. Characterization

2.3.1. Rheological measurement

Apparent melt viscosity was determined on an Instron Model 3211 capillary rheometer. The round die used had a length/diameter ratio of 40 and an entrance angle of 90°. Barel temperature was set at the range of 180–280 °C. Plunger speeds were 20, 6.0, 2.0, 0.6, 0.2 cm/min. Calculated hear rates varied from 10 to 1000 s^{-1}. Shear rates was calculated with (Eq. (1))

$$\tau_w = \frac{\Delta p}{2L/R} \quad (1)$$

where Δp is the pressure change, L is the length of the capillary and R is the radius of the capillary.

A modified Metzner form of the Rabinowitsch's equation (Eq. (2)) was used for calculating the shear rate

$$\dot{\gamma}_w = \frac{3n' + 1}{4n'} v \quad (2)$$

where the v was the speed of the plunger, $n' = \mathrm{d}\ln \tau_w / \mathrm{d}\ln \dot{\gamma}_{w,a}$ and $\dot{\gamma}_{w,a}$ is the shear rate at the wall, τ_w is the shear stress at the wall.

2.3.2. Scanning electron microscopy (SEM)

The samples of blend granules, composite fibers in cross and longitudinal sections for SEM were performed by chemical etching the minor phase (PS) of microtomed surfaces in xylene at room temperature for 2 h and then washed in freshly xylene and acetone to dissolve PS phase to obtain better contrast. All samples were dried and subsequently coated with a conductive gold layer and investigated by SEM (JEOL JSM-5600LV), operated at a working voltage of 10 kV.

An image analysis software MiVnt (Shanghai Quan Da Inc., China) was used to quantify the sizes of dispersed phases and their distribution in SEM micrographs. For each sample, two or three different images were examined. The perimeter and planar area of each structure in micrographs were quantified. Diameter calculated from the area of an equivalent circle for morphology of PS in microtomed surfaces. As such, a relevant average diameter, aspect ratio and standard deviation were obtained together with the dispersed phase size distribution in granules and each composite fiber.

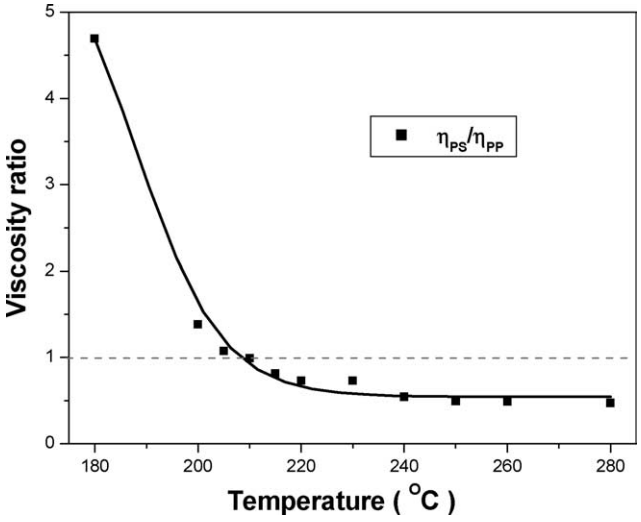

Fig. 1. Temperature dependence curves of viscosity ratio of PS to PP at a shear rate of 100 s^{-1}.

3. Result and discussion

3.1. Rheological properties of PP, PS and polyblends

The dependence of morphology on the viscosity ratio of dispersed phase to matrix ($p = \eta_d/\eta_m$) has earlier been investigated by Wu S. [4]. Theoretically, he found, while the other factors are the same, the component polymers with equivalent viscosity will be mixed well and generate the smallest particles after the blend process. Min K. et al. [27] reported for polyethylene/polystyrene (PE/PS) blends that when the dispersed phase had a lower viscosity it formed long ligaments in the matrix, but with higher viscosity the dispersed phase was in the form of discrete droplets. The formation of fibril in immiscible polymer blends is a course of dispersed phases deformation and orientation correlating with the viscous force and interfacial tension between the dispersed phase and matrix [28,29]. For good fibrillation to be achieved the viscosity of dispersed phase should be lower than that of the matrix (i.e. $\eta_d/\eta_m < 1.0$) [30] which has been reported in lots of investigations for FPM composites. Since, the viscosity of polymers strongly depends on the melt temperature and shear rate [31,32], the blend morphology could be designed by the rheological properties of dispersed phase, matrix and polyblend in the actual processing conditions.

Temperature dependence curves of viscosity ratio of PS to PP at 100 s^{-1} were shown in Fig. 1. The experimental results showed that the viscosity ratio was more than 1.0 below 210 °C and less than 1.0 above 210 °C, which approaching the constant about 0.5 with temperature increase. The viscosity ratio increased with shear rate rising as shown in Fig. 2. When temperature was above 230 °C, in the test range of shear rate, the viscosity ratio was always less than 1.0. And the sensitivity of viscosity ratio to shear rate reduces with temperature increased. In order to get the fibrillar PS morphology, the fiber processing conditions

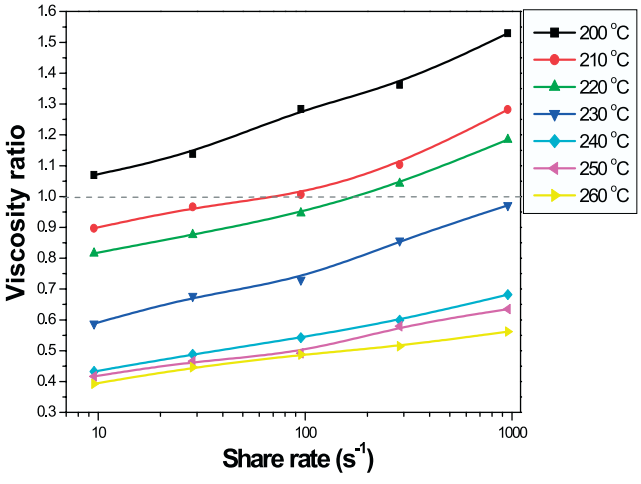

Fig. 2. Shear rate dependence curves of viscosity ratio of PS to PP at difference temperature.

should be determined at the operation window designed by temperature and shear rate, in which the viscosity ratio should be less than 1.0.

The rheological properties of polyblends are also relative to the blend composition. Fig. 3 showed viscosity as a function of composition at three different shear rates. At all shear rates, in the present work, appreciable negative deviation was noted from the value given by the simple additive rule of viscosity mixtures (Eq. (3))

$$\eta = w_{PP}\eta_{PP} + w_{PS}\eta_{PS} \tag{3}$$

where η, η_{PP} and η_{PS} are the apparent viscosities for the polymer blend, PP and PS, respectively, and w_{PP} and w_{PS} are the respective the weight fractions of the two components.

Negative viscosity deviation for immisciable polymer blends is associated with an increase in specific volume and voids at the interfaces [33]. And in this polyblend, the particles of dispersed phase become finer than those in the polyblend with positive viscosity deviation after the same processing [19]. The similar results for viscosity-composition dependences have been reported in PP/PA6 blends [19], PA66/PP blends [34] and HDPE/PA6 blends [35], respectively.

3.2. Morphology of PP/PS blend granules

The PP/PS blend granules for spinning were prepared by twin-screw extruder at 220 °C. As shown in Fig. 1, the η_{PS}/η_{PP} ratio was 0.65 (less than 1.0) which implied PS phase easily forming the fine particles in PP matrix. Fig. 4 gave the SEM images of microtomed surfaces, etched the PS phase, for 98/2, 96/4, 94/6 and 92/8 PP/PS blend granules. The black domains represented the position of the etched PS dispersed phase in PP matrix. As shown in Fig. 4, the PS phase was independently well dispersed in PP matrix with micron size in the different blends. Both the size and number of dispersed phase increased with the rising of PS content.

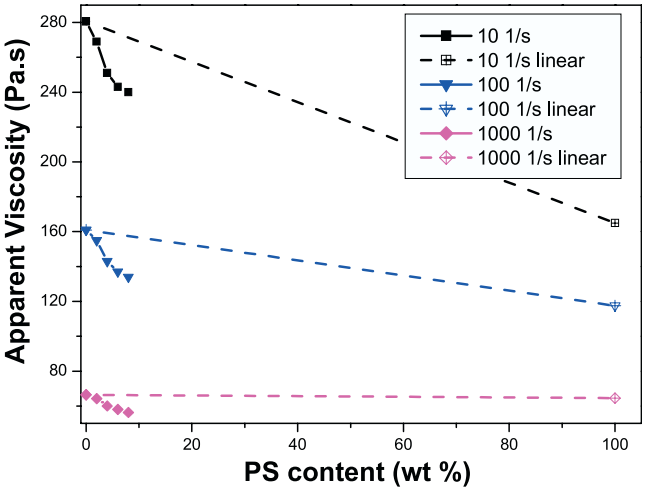

Fig. 3. Apparent viscosities of blends as a function of PS wt% content at different three shear rates, the PS wt% content for PP/PS blend shown in this graph is 0%; 2%; 4%; 6%; 8% and 100%.

Table 1 showed the statistical average size and the standard deviation of PS domain carried out with the image analysis software. When the amount of PS increased, the average size of minor phase changed from 0.77 μm (PS 2 wt%) to 1.20 μm (PS 8wt%) with the standard deviation slightly increased from 0.10 to 0.16 μm. The growth in d_n, as well as the width of size distribution undoubtedly results from flow-induced coalescence that occurred in blends of higher minor phase content prepared by melt mixing [36], and Han C. D. et al. [37,38] investigated the morphology evolution in mixer of PP/PS blend. He pointed out, while the mixing temperature was above the certain temperature and the η_{PS}/η_{PP} ratio was below the unit, the well-developed dispersed morphology could be observed and the blend ratio was predominant over the viscosity ratio in determining the morphology of PP/PS blend. This was consistent with our results. On the other hand, the relative deviations SD/d_n in different composition nearly kept the constant around 13%, implying that the relative size distributions of PS dispersed phase in polyblends were self-similar.

3.3. Morphology of PP/PS as-spun composite fibers

During the fiber formation, the PS deformation may take place in two main stages. Firstly, there was an elongational flow at the entrance spinneret hole, where deformation could take place. The shear flow tended to break up the polydomain structure, while extensional flow would consolidate and orient it [39]. Secondly, an elongational strain existed below the spinneret, which could deform the PS phase in fiber path.

According to Huneault et al. [40], drop deformation and break-up depend on the reduced capillary number, Ca^*, which is following (Eq. (5)):

$$Ca^* = \frac{Ca}{Ca_c} \tag{5}$$

where Ca is the capillary number and Ca_c is the critical capillary number.

The capillary number, Ca, depends on strain rate, elongational viscosity, and droplet size, expressed as Eq. (6).

$$Ca = \frac{\text{hydrodynamic stress}}{\text{interfacial stress}} = \frac{\eta_m \dot{\gamma} R}{\sigma} \tag{6}$$

where η_m is the matrix viscosity, $\dot{\gamma}$ the shear rate, R the drop radius, and σ the interfacial tension.

The critical capillary number, Ca_c, depending on the viscosity ratio, $p = \eta_d/\eta_m$. In the elongational flow, Ca_c is calculated from the Grace's empirical Eq. (7) [41]:

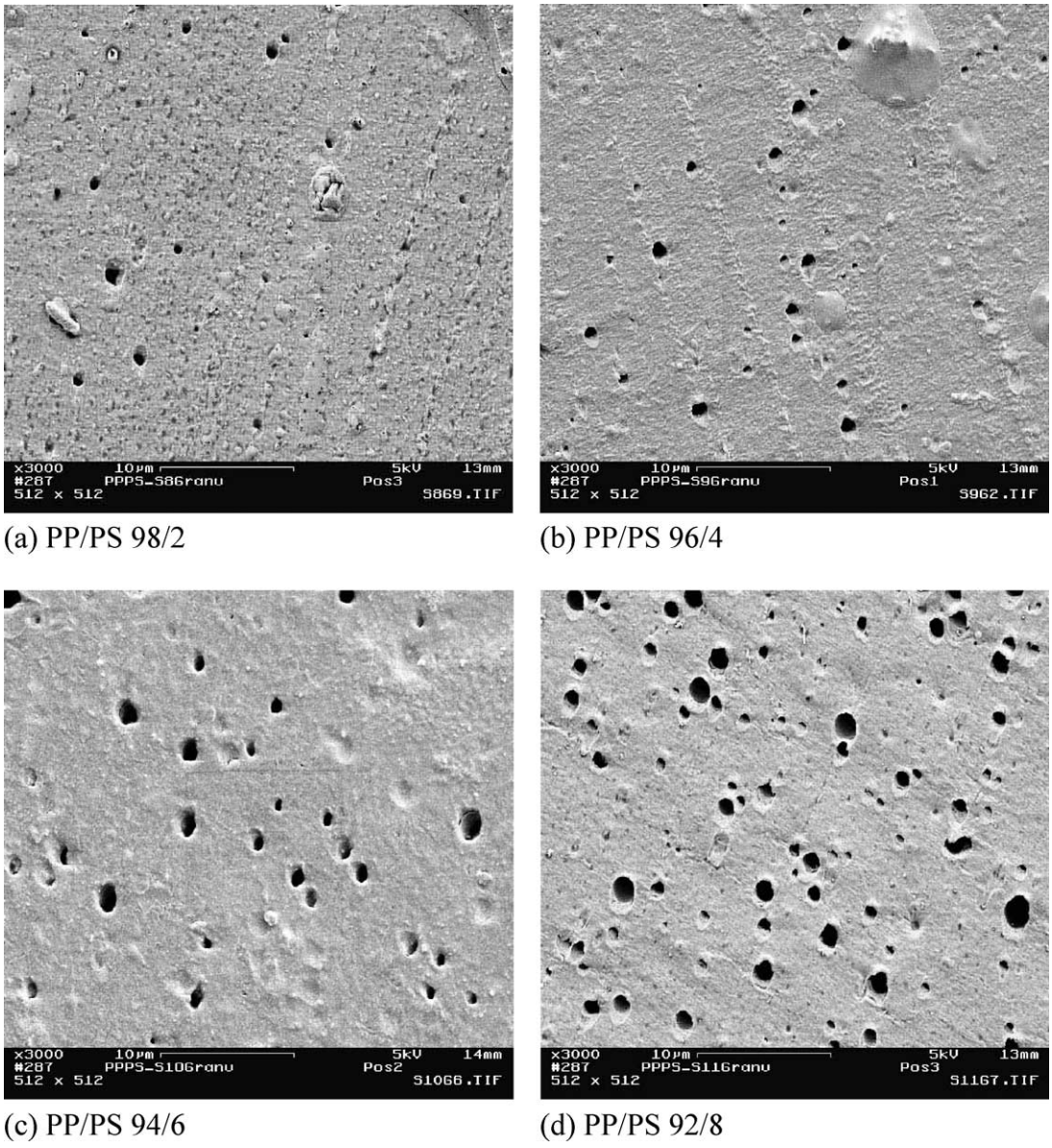

Fig. 4. SEM micrographs of PP/PS blend granules, (a) PP/PS 98/2, (b) PP/PS 96/4, (c) PP/PS 94/6, (d) PP/PS 92/8.

$$\log\left(\frac{Ca_c}{2}\right) = -0.64853 - 0.02442(\log p) + 0.02221(\log p)^2 - \frac{0.00056}{(\log p - 0.00645)} \quad (7)$$

Depending upon the value of Ca^* in both shear and elongation, the droplets will be either deformed or broken according to following criteria [40]:

1. If $Ca^* < 0.1$, droplets do not deform.
2. If $0.1 < Ca^* < 1.0$, droplets deform without break-up.
3. If $1.0 < Ca^* < 4.0$, droplets deform, but they break conditionally.

Table 1
Statistical analysis of spherical dispersed PS domain in polyblend granules

Sample code	Particle diameter, d_n[a] (μm)	Standard deviation, SD (μm)	Relative deviation, SD/d_n (%)
PP/PS (98/2)	0.77	0.10	12.99
PP/PS (94/6)	0.83	0.11	13.01
PP/PS (96/4)	1.13	0.15	13.32
PP/PS (92/8)	1.20	0.16	13.33

[a] d_n, the number particle diameter.

4. If $Ca^* > 4.0$, droplets deform affinely with the rest of the matrix and extend into long stable filaments, which deformation is calculated by the exponential function for uniaxial deformation.

For Ca^* between 0.1 and 4.0, the deformation is calculated by the linear deformation equation as suggested by Taylor (Eq. (8))

$$D = \mathrm{Ca}\frac{19p + 16}{16(p + 1)} \tag{8}$$

In the region $1.0 < Ca^* < 4.0$, the kinetics of the break-up depend on the viscosity ratio. The dimensionless break-up time (t_b^*) is calculated as (Eq. (9)) [42]:

$$t_b^* = \frac{t_b \gamma'}{\mathrm{Ca}} = 84p^{0.345}\left(\frac{\mathrm{Ca}}{\mathrm{Ca_c}}\right)^{-0.559} \tag{9}$$

where t_b is the time for break-up and γ' the strain rate. Break-up does not occur if there is not enough time provided for the break-up before solidification.

Fig. 5 showed the SEM micrographs of as-spun composite fibers in microtomed cross-section. It was clearly shown that different blend fibers were with the similar diameter about 20 μm. The big PS dispersed phase existed near to the surface and its number increased with more content of PS. Compared to 98/2 and 96/4 fibers, the big PS domains were substituted by the much smaller ones in the center of 94/6 and 92/8 ones. In this case, each cross-section of fiber was divided five cirque parts along the radial direction with the same distance about 2.0 μm except the cirque near to the surface since, the different blend fiber diameter. Then the different average diameter of PS phase was tested by the image analyzer and plotted with the distance along radial direction to get the Fig. 6. And the 2D dispersed phase distribution in as-spun fiber cross-section was obviously shown in it. The size of dispersed phase gradient increase existed in Fig. 6 (trace of 6 and 8 wt% PS), but in the other two kinds of fibers there was no evident difference from fiber center to surface. It implied that the composition of PP/PS not only affected the size of PS in fiber cross-section, but also brought the morphology structure transformation in fiber center. In former studies, the dispersed phase distribution in blend fiber cross-section was often neglected especially in fine fiber due to the difficult characterization.

In order to investigate the 3D morphology of dispersed phase in composite fibers, the SEM micrographs of fiber in microtomed longitudinal section were exhibited in Fig. 7.

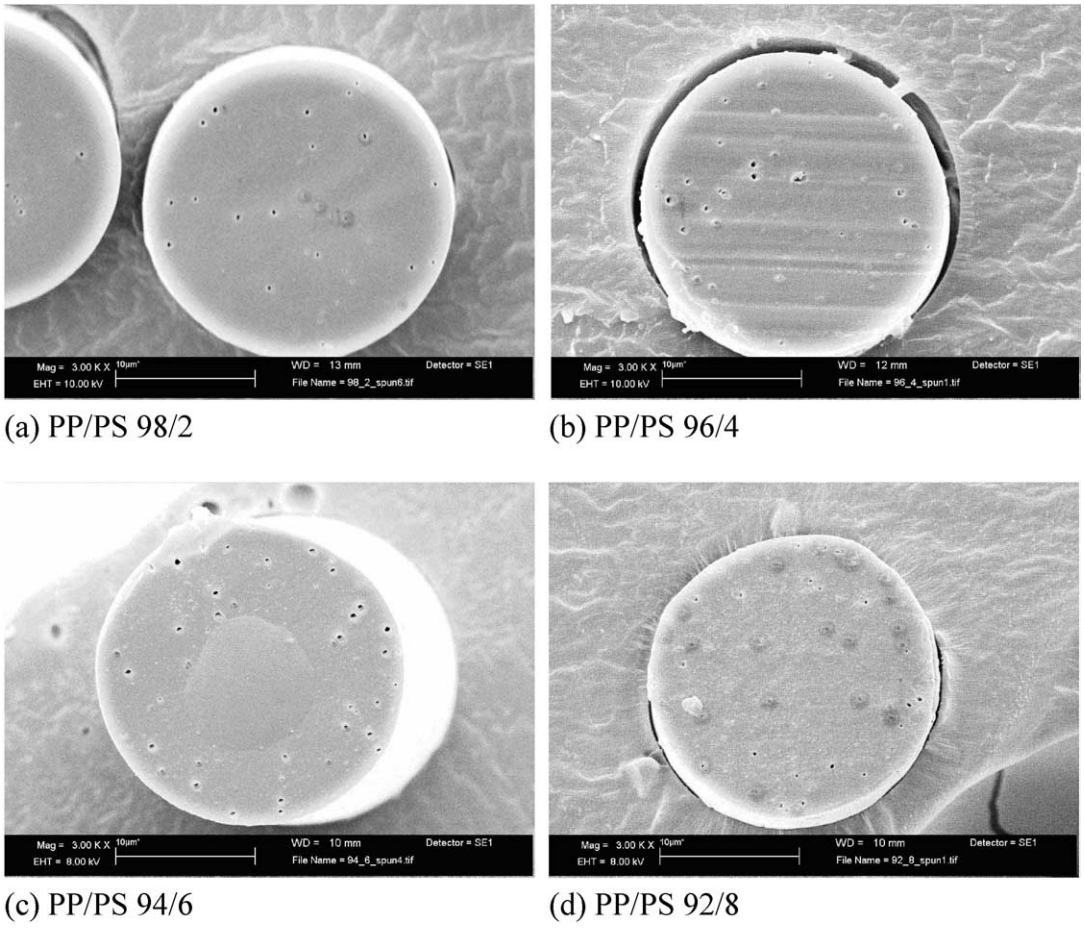

Fig. 5. SEM micrographs of PP/PS as-spun composite fibers in cross-section. (a) PP/PS 98/2, (b) PP/PS 96/4, (c) PP/PS 94/6, (d) PP/PS 92/8.

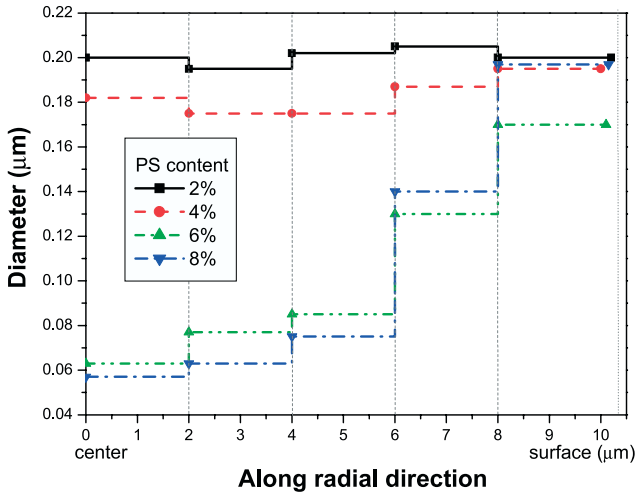

Fig. 6. Plot of average PS phase diameter vs. distance along radial direction in PP/PS as-spun composite fibers cross-section.

From these images and cross-section SEM in Fig. 5, there was an obvious conversion of dispersion morphology. At lower PS content (2 and 4 wt%), the PS phases was near ellipses along the longitudinal direction with similar short axis in about 200 nm and lower aspect ratio (*L*/*D*) 1.5–5 (Fig. 7(a) and (b)). In the 8 wt% PS composite fiber (Fig. 7(c)), nano-scale (50–70 nm) fine fibril morphology was distinctly observed in fiber center. These suggested the formation of fibrillar phase morphology was also related to the dispersed phase concentration. At the present spinning process, a critical dispersed phase concentration for fibril formation existed at PS 4 wt%. The limited dispersed phase amount for FPM was also reported in investigations for TP/LCP in situ composites [43] and HDPE/PA6 blends under extensional flow [28]. During preparation of the SEM samples, if the cut deviated somehow from the ideal fiber longitudinal direction, which effected on the PS shape in the SEM images that could not show the actual PS morphology in PP fiber along the longitudinal direction. In this work, the deviated cutting angles to the ideal direction were less than 5°, which were calculated with the SEM micrographs of fiber section shape. The influence on the PS shape brought from the cutting can be ignored and the PS morphology size in the PP fiber can be deemed to reveal in the SEM images.

In Figs. 6 and 7(c), it especially exhibited gradient PS phase structure in composite fibers. That was, along the fiber radial direction in PP/PS (92/8) composite fiber, the nano-scale fine fibrils became bigger from 50–70 nm to 200 nm, and the aspect ratio (*L*/*D*) reduced from above 50 (about 3 μm length) to below 10 (below 2 μm length). The 'thin

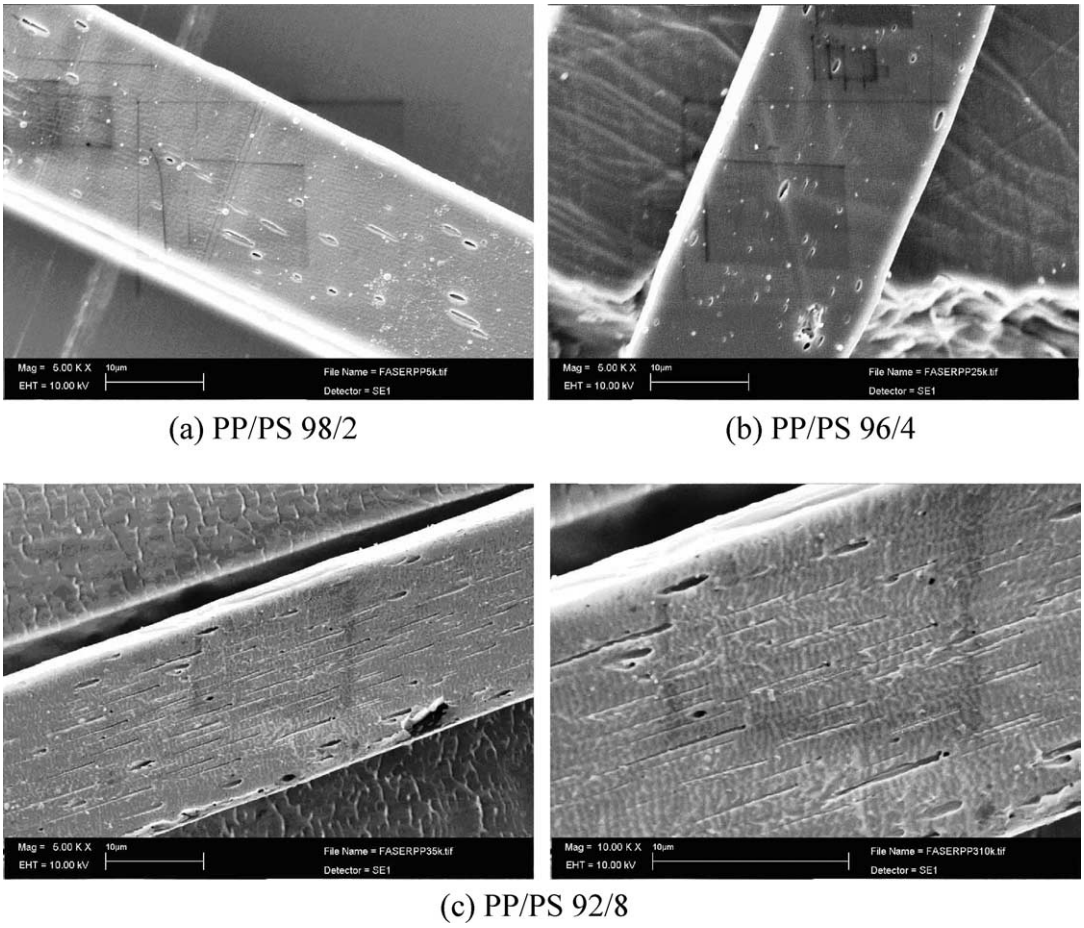

Fig. 7. SEM micrographs of PP/PS as-spun composite fibers in longitudinal section, (a) PP/PS 98/2, (b) PP/PS 96/4, (c) PP/PS 94/6.

and long' phase evolved to 'fat and short' phase. In Kotek R. et al. [19] investigation, the fibrils were found to be located mainly in the core of filaments and oriented in the direction of fiber axis. While Tsebrenko et al. [44] reported the fibrils formed in the region, where the polymer exited the capillary and they were dispersed uniformly in the cross-section of the fiber. All of these were not mentioned the 2D gradient distribution as this work.

According to study on the morphology of polyblend granules in Section 3.2, it was reasonable that PS phases in blend melt were relatively uniform in size before the spinneret entrance. The PS phase morphology transformation from center to surface was due to the different deformation, break-up and coalescence process in fiber radial direction during the fiber formation. It can be divided to two parts: (A) the 'pipe surface' effect on the blends melt flow in spinneret; (B) the variation gradient distribution along the radial direction of fiber during spinning path.

In the spinneret, there was a gradient elongational stress from center to surface which induced the distribution of Ca calculated as Eq. (6) in polyblend melt. While at the processing temperature 260 °C, the viscosity ratio p was lower sensitive to stress as shown in Fig. 2. Therefore, the Ca_c from Eq. (7) did not have the same distribution as Ca. So the Ca^* existed the difference along the radial direction in spinneret which implied the different PS droplets deformation in spinneret melt flow field. And since, the length spinneret was 1 mm, existing time of melt flow in spinneret was short which also suggested the lower PS droplets deformation and limited 2D deformation distribution in cross-section.

In the former study on in situ composite fibers, the dispersed phase fibrils mainly occurred after the spinneret. The fibril morphology in fibers was obviously controlled by the take-up speeds or the drawn ratios [11]. Nearly all of the investigations were about the fibers by drawing the extrudate from the screw extruder die and few of them mentioned the fine composite fibers with 20 μm diameter. Isayev A. I. et al. [45] simulated the LCP droplet deformation in fiber spinning of self-reinforced composites. The calculated LCP fibril diameter in matrix by affine deformation theory was well matched to the observation by SEM and the image analyzer. But their simulation was performed based on negligible radial temperature profile in melt spinning, bigger die diameter for fiber formation about 10 mm and lower take-up speed <100 m/min. While in the common fiber formation with much smaller spinneret and higher spinning speed, the fiber path is a complicated process from polymer melt to solid. The radial variation such as temperature profiles, axial velocity and stress in fiber spinning define the fiber structures and properties. The 2D or 3D models [46,47] for melt spinning of polymers have been set up to corrected the 1D model, with axial velocity, stress and temperature assumed to be uniform across all cross-sections [48]. These models significant revealed the one component polymer spinning process and the relationship to the thin fiber structure, such as crystallization and orientation. And the radial variation would induce the difference in fiber cone and skin, which was influenced by the spinning conditions, such as temperature, take-up speed. In this case, the gradient PS morphology was intensively controlled by the radial variation during fiber path.

At the spinneret exit the Ca^* calculated by Eq. (5) was larger than 4.0, which implied the PS droplets would deform to the fibrils. The whole calculated method was according to the Isayev A. I. work [45] and the interfacial tension was estimated using the surface tension of two components [49]. After the spinneret, the blend melt diameter rapidly decreased in the melt zone and went into the solid zone with a constant lower diameter to form the as-spun blend fiber by take up stress. During this process range, the blend temperature changed from 260 °C to room temperature, while the blend viscosity, viscosity ratio, interfacial tension and axial stress were intensively related to it. And the Ca^* reduced with the increasing of distance from the spinneret for the temperature continuously decreasing. If the 1D model for melt spinning was used to simulate this range, the different Ca^* could be calculated theoretically to get a numeral analysis as shown in former work [45]. While in qualitative analysis combing the former calculated Ca^* at the spinneret exit, it was an acceptant result that the Ca^* transformed form above 4.0 to below 0.1, which revealed the different PS phase deformation stage in different distance from the spinneret. Furthermore, if the 2D melt spinning model was taken into account at a certain point in the fiber path, the radial variation brought the radial Ca^* deviation which determined the size distribution of PS phase in fiber cross-section. Compared to the fiber surface, the core has higher temperature, lower viscosity and longer solidification time [47,48], which suggest the PS has the more deformation degree than that near to the surface. It was one of the most important reasons that the gradient PS phase morphology was formed in composite fibers.

The above mentions just discussed the deformation of PS phase but ignored its coalescence and break-up in fiber formation. The deformation, break-up and coalescence are three interrelated factors and decide the final dispersed morphology structure, which have been widely investigated in multiphase polymer blend mixing process, but fewer was mentioned in blend fiber formation. Kotek R. [19] reported the PA6 droplets coalesced during melt spinning which led to the development of fibril morphology. And the simulation of break-up of LCP phase during fiber spinning of the blend based on the dimensionless break-up time indicated the absence of their break-up [45]. All of these works were based on the lower take-up speed and bigger diameter fiber, which would bring some difference to thin fiber formation. In this case, if the PS phase with uniform volume at the spinneret exit just deformed and no break-up or coalescence presented during the fiber path, the PS fibrils in final fiber should have same uniform volumes. In this work, the PS phase in fiber was assumed to have a cylindrical shape and

its volume will be given by Eq. (10)

$$V = \pi R_f^2 L_f \tag{10}$$

where R_f is the number average radius of fibril and L_f is the length of the fibril.

The different R_f and L_f of PS phase in the fiber from center to surface was measured by image analyzer. According to the calculated result, the PS volume approaching the fiber surface was five times more than that in the core. It suggested the presence of radial difference coalescence or break-up. As the higher viscous matrix, longer contact time required for coalescence and bigger density difference between droplets and matrix will reduced the coalescence [36,50]. During the spinning path, the faster temperature reducing, higher axial velocity and stress brought the higher viscosity and lower contact probability and time for dispersed phase coalescence. Therefore, the coalescence in this fiber with higher take-up speed was limited. Especially near to the fiber surface, the radial temperature induced the higher viscous and lower PS phase deformation. And the coalescence of PS phase became more difficult than it in the core and nearly remained the former volume. On the other hand, the bigger PS phase deformed to the fibril with higher L/D, the easier it broke up. In this case, the PS was an amorphous polymer with poor adhesive ability and higher interfacial tension to PP matrix. So the nano-scale PS fibril in PP matrix was unstable and would easily break up at a very small fluctuation, for its higher surface energy and lower diameter. During the fiber processing, the transformation of the processing fields and properties of PP matrix provided the break-up morphology,

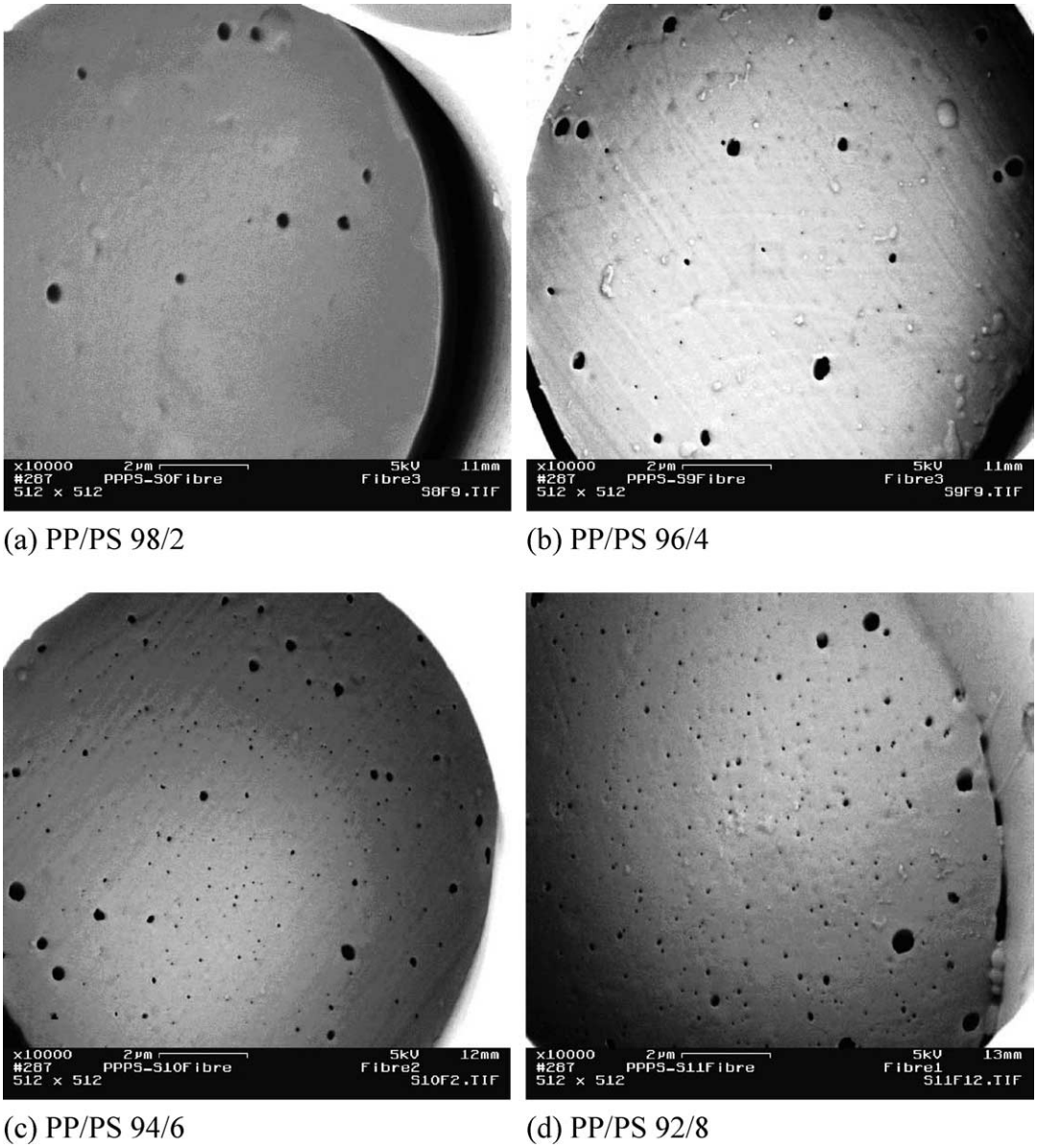

Fig. 8. SEM micrographs of PP/PS drawn composite fibers in cross-section. (a) PP/PS 98/2, (b) PP/PS 96/4, (c) PP/PS 94/6, (d) PP/PS 92/8.

especially in the fiber center. It was also consistent with the Ca^* evolution above mentioned.

3.4. The morphology of PP/PS drawn composite fibers

Post-drawing for the as-spun fibers is a common process to change the orientation and crystal structure of final drawn fiber and brings its good and stable properties. In this work, the PP/PS drawn fibers were made through the as-spun fibers after hot-drawn with 3 times draw ratio. As shown in Section 2.2, the drawn temperature was above the T_g of PP and PS which suggested the two components could occur the solid deformation and change the morphology structure of composite fibers. Fig. 8 showed the dispersed phase morphology of the composite drawn fibers in cross-section. Compared to Figs. 5 and 8, the diameter of fibers decreased obviously from 20 μm (as-spun fiber) to 12 μm (drawn fiber), but the size of the PS phase in cross-section slightly reduced after the hot-drawing. It showed the present drawing process can not effectively deform the solid dispersed phase, owing to the drawn stress was difficult to transfer from matrix to dispersed phase through the solid interface, and the free space allowing the PS phase deformation was limited.

The image analysis software MiVnt was used to analyze SEM images for the distribution of PS of drawn fibers in cross-section. Each cross-section of fiber was divided four cirque parts along the radial direction with the same distance about 1.5 μm as the former investigation in as-spun fibers. Fig. 9 showed the change of average PS phase diameter vs. distance along radial direction. The gradient phase structure was also intensively related with PS content, similar as it in the as-spun fibers in Section 3.2. In composite drawn fibers with 6 and 8 wt% PS, the 2D nano-scale diameter PS domains also appeared near to the surface besides the bigger ones as shown in Fig. 8(c) and (d), compared to as-spun fibers in Fig. 5(c) and (d). It induced the lower average size of dispersed phase (shown in Fig. 9) and higher standard deviation (shown in Fig. 10) near to the surface in these fibers. In their center area, the standard deviation was much lower, which suggested the uniform sizes of PS phase with 2D nano-scale. However, in the 2 and 4 wt% PS composite drawn fibers as shown in Fig. 10, the lower standard deviation was near to the surface coursed by the lower number of PS domain, and the higher standard deviation was in the center brought by the larger size of PS phase. In the post-drawing process, the diameter of fiber reduced through the orientation, transformation and rearrange of PP matrix amorphous, mesophase and crystal along the fiber axial direction. At the same time, the PS dispersed phase slipped with PP matrix deformation which formed the new distribution as above mentioned results.

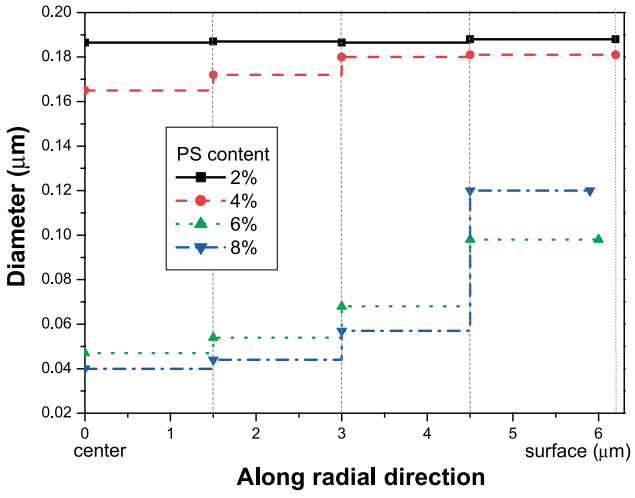

Fig. 9. Plot of average PS phase diameter vs. distance along radial direction in PP/PS drawn composite fiber cross-section.

4. Conclusions

The component properties and blend ratio were two important factors that influenced the morphology of the PP/PS polyblends. The viscosity ratio of PS to PP varied from above 1.0 to below 1.0 with the temperature and shear rate increase. And the polyblends showed the negative viscosity deviation from the value calculated by the simple rule of mixtures in the test region. The size (d_n) and its standard deviation (SD) of dispersed PS phase increased with an increasing of PS amount. The relative deviations (SD/d_n) in different blends nearly kept the constant around 13%. After melt spinning process, the different size and the distribution of dispersed phase morphology were showed in as-spun composite fibers. The average 2D sub-micron ellipse dispersed morphology existed in fibers with 2 and 4 wt% PS, while the gradient nano-scale fibril morphology along the radial direction were shown in fibers with 6 and 8 wt% PS. The gradient nano-scale fibril morphology in

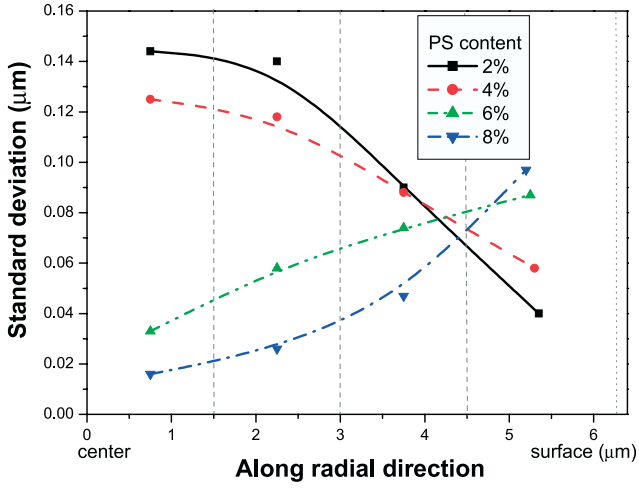

Fig. 10. Plot of standard deviation of average PS phase diameter vs. distance along radial direction in PP/PS drawn composite fiber cross-section.

as-spun fibers was attributed to the radial variation such as temperature, viscosity, axial velocity and stress in spinning path and the different break-up and coalescence of dispersed phase from fiber center to surface. It was also in agreement with the results analyzed according to droplet deformation criteria based on the reduced capillary number. Furthermore, the post hot-drawing process slightly reduced the 2D sizes of PS phase and influenced its distribution in fiber cross-section, but distinctly reduced the diameter of the composite fiber. This investigation of the relationship between the processing technology and morphology can provide a guideline for the design, research and development of new nano-polymer composite fibers.

Acknowledgements

The authors thank the National High-tech 863 Project (2002AA302616), the National Natural Science Foundation of China (20174003), the Shanghai Nano Special Project (0219 nm039), and the Shanghai Nanotechnology Application Plateform (0359 nm008) for the financial support as well as the program '211 Engineering' of the 'Tenth Five Plan'.

References

[1] Varga J, Breining A, Ehrenstein GW. Int Polym Proc 2000;XV:53.
[2] Song CH, Isayev AI. J Polym Eng 1998;18:417.
[3] Kiss G. Polym Eng Sci 1987;27:410.
[4] Wu S. Polym Eng Sci 1987;27:335.
[5] Heino MT, Hietaoja PT, Seppala JV. J Appl Polym Sci 1994;51:259.
[6] Jin X, Li W. JMS Rev Macromol Chem Phys 1995;C35(1):1.
[7] Lee MW, Hua X, Yue CY, Li L, Tamb KC. Compos Sci Technol 2003;63:339.
[8] Sayant S, Sauvarop B-L, Geoffrey RM, Robert HO. Polymer 2003;44:3407.
[9] Wang HM, Tao XM, Newton E, Chung TS. Polym J 2002;34:575.
[10] Varma DS, Dhar VK. Tex Res J 1988;58:274.
[11] Grasser W, Schmidt HW, Giesa R. Polymer 2001;42:8517.
[12] Qiao F, Milger KB, Hunston DL, Han CC. Polym Eng Sci 2001;41:77.
[13] Vallejo FJ, Eguiazabal JI, Nazabal J. Polymer 2000;41:6311.
[14] Sukananta P, Bualek-Limcharoen S. J Appl Polym Sci 2003;90:1337.
[15] Qin Y, Brydon DL, Mather PR, Wardman RH. Polymer 1993;34:1196.
[16] Qin Y, Brydon DL, Mather PR, Wardman RH. Polymer 1993;34:1203.
[17] Qin Y, Brydon DL, Mather PR, Wardman RH. Polymer 1993;34:3597.
[18] Liang BR, White JL, Spruiell JE. J Appl Polym Sci 1984;51:259.
[19] Afshari M, Kotek R, Kish MH, Dast HN, Gupta BS. Polymer 2002;43:1331.
[20] Takahashi T, Konda A, Shimizu Y. Sen-i-Gakkaishi 1996;52:507.
[21] Grof I, Durcova O, Jambrich M. Colloid Polym Sci 1992;270:22.
[22] Lyoo WS, Chai YG, Ha WS, Kim BC. Int Polym Process 2000;XV:369.
[23] Jones FR. Handbook of polymer–fiber composites. Essex: Longman Scientific and Technical; 1994. p. 279.
[24] Harmia T, Fredrich K. Compos Sci Technol 1995;53:423.
[25] Yu CB, Zhu MF, Chen YM. J Appl Polym Sci 2001;82:3172.
[26] Zhu MF, Yan WD, Lu Y, Chen YM, Adler HJ, Poetschke P, et al. Macromol Symp 2001;164:369.
[27] Min K, White JL, Fellers JF. Polym Eng Sci 1984;24:1327.
[28] González-Nuñeza R, Moscoso FJ, González-Romero VM, Favis BD. Polymer 2001;42:5485.
[29] Hemmati M, Nazokdast H, Panahi HS. J Appl Polym Sci 2001;82:1129.
[30] Kim BK, Do IH. J Appl Polym Sci 1996;60:2207.
[31] Wang HM, Lee KW, Chung TS, Jaffe M. Polym Compos 2000;21:114.
[32] Fang ZP, Ma GW, Shentu BQ, Cai GP, Xu CW. Eur Polym J 2000;36:2309.
[33] Plochocki AP. Polym Eng Sci 1983;23:618.
[34] Park SJ, Kim BK, Jeong HM. Int Polym J 1990;26:131.
[35] Hietaoja PT, Holsti-Miettinen RM, Seppala JV, Ikkala OT. J Appl Polym Sci 1994;54:1613.
[36] Sudararaj U, Macosko CW. Macromolecules 1995;28:2647.
[37] Lee JK, Han CD. Polymer 1999;40:6277.
[38] Lee JK, Han CD. Polymer 2000;41:1799.
[39] Cheremisinoff NP. Handbook of engineering polymer materials. New York: Marcel Dekker; 1997. p. 585.
[40] Huneault MA, Shi ZH, Utracki LA. Polym Eng Sci 1995;35:115.
[41] Grace HP. Chem Eng Commun 1982;14:225.
[42] Utracki LA, Shi ZH. Polym Eng Sci 1992;32:1824.
[43] Beery D, Kenig S, Siegmann A. Polym Eng Sci 1996;36:229.
[44] Tsebrenko MV, Yudin AV, Ablazova TI, Vinogrdov GV. Polymer 1976;17:831.
[45] Song CH, Isayev AI. Polymer 2001;42:2611.
[46] Henson GH, Bechtel SE. Int Polym Proc 2000;XV:386.
[47] Henson GH, Cao D, Bechtel SE, Forest MG. J Rheol 1998;42:329.
[48] Schultz WW, Davis SH. J Rheol 1982;26:331.
[49] Van Krevelen DW. Properties of polymers—the estimated and correlation with chemical structure. Amsterdam: Elsevier; 1981. p. 34.
[50] Fortelný I, Kovár J. Polym Compos 1988;9:119.